

Electric field induced enhancement of photovoltaic effects in graphene nanoribbons

Sara Zamani and Rouhollah Farghadan*

Department of Physics, University of Kashan, Kashan, 87317-53153, Iran

(Received 8 January 2019; published 17 June 2019)

The terahertz (THz) to visible irradiation induced current in zigzag and armchair graphene nanoribbons were investigated by focusing on the modulation of the photovoltaic effects by tuning the electric field (E) strength. The numerical results show that spin photovoltaic effects in zigzag-edged graphene nanoribbons can be significantly improved by enhancing the E strength. In detail, an acceptable broadband photoresponsivity with a full optical spin polarization in a broad range of photon energies, including the THz region, can be obtained that can be preserved in the presence of the edge roughness. Furthermore, armchair-edged graphene nanoribbons could reveal a tunable photoresponsivity induced by THz to ultraviolet wavelengths. These results could lead to the enhancement of photovoltaic effects and especially the generation of a spin-polarized photocurrent in all-carbon junctions.

DOI: [10.1103/PhysRevB.99.235418](https://doi.org/10.1103/PhysRevB.99.235418)**I. INTRODUCTION**

Recently, spin-photovoltaic properties of graphene nanostructures have attracted much attention thanks to their long spin-relaxation length, ballistic quantum transport, high carrier mobility [1,2] and excellent optoelectronic properties including an ultrafast saturable absorption, a broadband photoresponsivity, a low dissipation length, etc. In this regard, some studies have been conducted, in which spin-polarized photocurrents have been realized in graphene nanostructures through several approaches including the spin injection from ferromagnetic contacts [3,4], the optical orientation process [5–7], the intrinsic magnetization of the nanostructures [8], the staggered potential of the hBN/graphene heterostructure [9], or by applying a magnetic field [10]. Among various graphene nanostructures, graphene nanoribbons (GNRs) seem appealing for spin-photovoltaic applications due to their feasible synthesis methods including cutting from carbon nanotubes, bottom-up approaches, and lithography techniques [1,11–14] as well as due to the modification of various properties of the pristine graphene, for example, a nonzero band gap, resulting from the quantum confinement effect and edge states [15]. Furthermore, GNR-based field-effect transistors (FETs) and photodetectors have been fabricated previously [16–18]. GNRs exist in two shapes: nonmagnetic (NM) armchair-edged GNRs (AGNRs) and zigzag-edged GNRs (ZGNRs) with an antiferromagnetic (AFM) ground state [19] with a band gap that is inversely proportional to the ribbon width [20]. The spin characteristic of ZGNRs originates from the electron-electron interaction and can be tuned and converted to the half-metallicity state by modifying the edges [8,19–21], by doping through the adatom adsorption [9,22,23], by creating point/line defects [24,25], and by applying an external perturbation such as a magnetic field [10] a transverse electric field [20,26], or an inhomogeneous bias [27].

On the other hand, by applying an external transverse electric field on an AFM ZGNR, the edge-state band gap of one spin orientation closes while the edge-state band gap of the other spin orientation widens, resulting in the breaking of the ZGNR spin degeneracy and thus a half-metallic behavior under an appropriate field strength [20,28,29]. Furthermore, in a NM AGNR, electronic properties could be modulated by applying an external transverse electric field [30], as reported previously [30–32]. However, as opposed to ZGNR, the bands around the Fermi level do not belong only to the edge states, but they are associated with the wave functions distributed throughout the nanoribbon width.

Due to the strong dependence of GNR properties on the edge states, the electromagnetic behavior of GNRs under the effect of a transverse electric field was also investigated for various edge roughness. Generally, edge defects could affect the performance of graphene-based devices [24,25,33]. Vacancy defects reveal flat bands in the band structure of graphene with localized magnetic moments [34]. Furthermore, the edge magnetism in ZGNRs has been experimentally and theoretically confirmed at room temperature in the presence of atomic-scale edge defects [19,20,35] and also under the effect of both a transverse electric field and the edge disorder [20]. In the presence of edge defects, the qualitative behavior remains the same as that in the perfect GNR; however, the strength of some features, such as the spin polarization, decreases [19,35]. A previous study on the simultaneous effect of a transverse electric field and the 558-defect line on GNR showed a better spin polarization in the presence of the defects [36]. The polarization-induced switching effect in graphene nanoribbon edge-defect junction with a transverse electric field has also been proposed [37]. Interestingly, spin carriers of the ferromagnetic sawtooth-like GNR become spatially separated under a transverse electric field [19]. Furthermore, the linear and quadratic dependence of the band gap on the externally applied transverse electric field has been found for a jagged GNR with armchair and zigzag edges [38]. The effect of an electric field on electromagnetic and transport

*rfarghadan@kashanu.ac.ir

properties of heterostructures such as AGNR/BNNR (boron-nitride nanoribbon) and ZGNR/BNNR has also been investigated [39,40]. Additionally, periodic line defects could change the graphene conductivity and local point defects can change its absorption properties [41].

Although electronic and spintronic properties of GNRs with different edge terminations and applied transverse electric fields have been investigated considerably, their photovoltaic and spin-photovoltaic properties under a transverse electric field have been neglected. In previous studies, terahertz (THz) optical properties of graphene, including its optical refractive index, reflectivity, and conductivity, under an external longitudinal dc electric field [42] and optical properties of graphene under an electric field perpendicular to the graphene planes have been investigated [43]. In this paper, using the self-consistent nonequilibrium Green's function (NEGF) formalism and the mean-field Hubbard model, we theoretically simulated the electric field induced spin-polarized photocurrent in a spin-photovoltaic device based on pristine and defective GNRs illuminated with monochromatic linearly polarized irradiation with energies from THz to ultraviolet (UV). Our results showed that full (100%) and nearly full optical spin-filtering features are revealed in the illuminated ZGNRs under a transverse electric field. By tuning the electric field strength, one could broaden the range of photon energies with the full optical spin-filtering feature as well as decrease the threshold photon energy, where this feature starts, to achieve a fully spin-polarized photocurrent in the THz region of the electromagnetic spectrum. Graphene-based photodetectors operating under the THz radiation have been previously studied theoretically [5,44] and experimentally [45]. However, we indicated the electric field tunable photoresponsivity of GNRs as well as the full spin polarization characteristic of ZGNR under the THz radiation. To study the robustness as well as the strength of the spin-polarized behavior in the presence of edge defects, we simulated the electric field induced spin-polarized photocurrent in a defective ZGNR, which confirms the stability of the spin-dependent behavior of the nanodevice and also the reversing of the sign of the optical spin polarization in the THz to infrared range. Finally, we investigated the effect of an applied transverse electric field on transport properties and optical responsivity of the nanodevice, which is based on a semiconducting AGNR, and the numerical results reveal the photoresponsivity in photon energies ranging from THz to UV by properly tuning the electric field strength.

II. MODEL AND METHOD

The effect of an externally applied transverse electric field (E) on optoelectronic properties of the proposed nanodevice based on GNRs (depicted in Fig. 1) is simulated using the single-band first-order tight-binding approximation with the NEGF formalism as well as the Hubbard approximation in the case where ZGNR is the channel. The total Hamiltonian of the simulated nanodevice, including the effects of E and light irradiation, can be written as [46]

$$H_{T,\sigma} = H_{0,\sigma} + H_{e-ph,\sigma}, \quad (1)$$

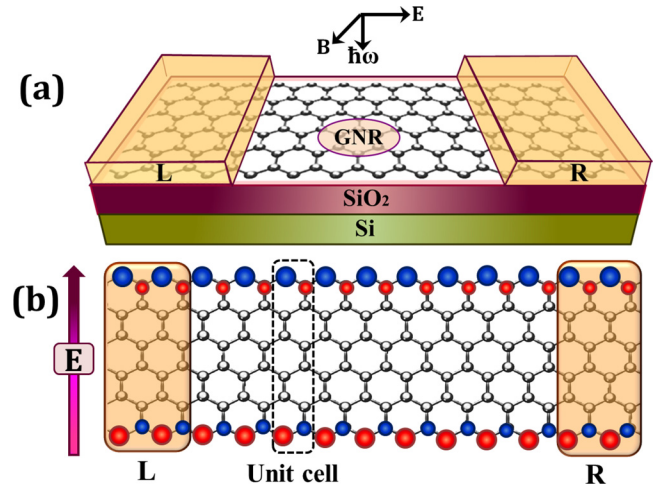


FIG. 1. (a) A schematic representation of the proposed nanodevice based on GNRs illuminated with linear radiation with a polarization that is parallel to the channel direction. (b) A schematic representation of n ZGNR ($n = 6$ denotes the number of zigzag chains along the width direction) under a transverse electric field. The dotted-line rectangle box denotes the ZGNR unit cell.

In the equation above, $H_{0,\sigma}$ indicates the Hamiltonian of the proposed nanodevice in the presence of E and in the absence of light irradiation. The term $H_{e-ph,\sigma}$ incorporates the interaction of light with the matter and it is treated as a perturbation Hamiltonian. Our simulation consists of two self-consistent calculations; first, taking into account the GNR electronic properties as well as magnetization (only for ZGNR) via the Hubbard approximation and second, calculating the interaction of light with the matter using the NEGF formalism.

A. Tight binding Hamiltonian and electron-electron interaction

The tight-binding Hamiltonian of a GNR in the presence of an external E and the electron-electron interaction can be written as [26,47]

$$H_{\sigma} = \sum_{\langle i,j \rangle, \sigma} -t d_{i,\sigma}^{\dagger} d_{j,\sigma} + \sum_{i,\sigma} eE(y_i - y_m) \hat{n}_{i,\sigma} + U \sum_{i,\sigma} \langle \hat{n}_{i,-\sigma} \rangle \left[\hat{n}_{i,\sigma} - \frac{1}{2} \langle \hat{n}_{i,\sigma} \rangle \right], \quad (2)$$

where $d_{i,\sigma}$ and $d_{i,\sigma}^{\dagger}$ are the electron annihilation and creation operators, respectively, and $\langle \hat{n}_{i,\sigma} \rangle$ is the expectation value of the number operator for an electron with the spin σ ($\sigma = \alpha, \beta$) at the site i . Furthermore, $\langle i, j \rangle$ denotes the summation over all nearest-neighbor sites and $t = 2.6$ eV is the transfer integral between the nearest-neighbor sites [26]. The second term in the equation above is the potential energy of E , where e is the electron charge, y_i is the position of the i th atom along the transverse direction of ZGNR, and y_m is the middle transverse position in the ribbon. Here, we neglected the depolarization field, which screens the external field. The third term in the equation above calculates the electron-electron interaction by self-consistently solving the Hubbard repulsion treated in the mean-field approximation [48], which results in

the emergence of the spin-resolved band structure of ZGNR. Note that the term $U = 2.75$ eV is the on-site Coulombic repulsion strength [26], which is revealed only in the simulation of the edge magnetism in ZGNRs, not in NM AGNR for which the Hamiltonian includes only the first two terms of Eq. (2).

The Hamiltonian of the proposed nanodevice contains the effect of left (L)/right (R) electrodes and also the applied E , can be decomposed as [49]

$$H_{0,\sigma} = H_{C,\sigma} + H_{R,\sigma} + H_{L,\sigma} + H_{RC} + H_{LC}, \quad (3)$$

where the first three terms described in Eq. (2) are the Hamiltonians of the channel, the right and left contacts, respectively. $H_{(L/R)C}$ represents the tight-binding Hamiltonian of the coupling between the channel and the L/R contact. Furthermore, to avoid the conductivity mismatch problem at the interface, we considered the same structure for the channel, the left and right contacts, and applied the external electric field on the whole nanodevice. Electronic properties, including the band structure and the density of states of the GNR-based nanodevice, were simulated using Eqs. (2) and (3) together with the mean-field Hubbard approximation in the case of ZGNR [48]. Taking into account the localized edge magnetism by the electron-electron interaction is the origin of the spin-dependent behavior of electronic properties in ZGNRs. Applying E results in different shifts of the energy levels at different atomic sites due to the addition of the related potential energy in the on-site terms of the Hamiltonian, which leads to different occupation numbers and hence different mean-field Hubbard terms. Next, using the self-consistent solution, we obtained the electric field induced spin-polarized band structure of ZGNR. After solving the Hamiltonian of the GNR channel and the left and right contacts, the retarded Green's function of the system, in the absence of light radiation, can be expressed as [49]

$$G_{0,\sigma}(\varepsilon) = [(E + i\eta)I - H_{C,\sigma} - \Sigma_{L,\sigma} - \Sigma_{R,\sigma}]^{-1}, \quad (4)$$

where I is the identity matrix, η is an infinitesimal broadening, and $\Sigma_{(L/R),\sigma}$ denotes the self-energy of the L/R contact, which contains the influence of the electronic structure of the L/R electrode through the Green's function of the electrode's surface, and it is computed using the Sancho iterative approach [48,50]. By solving Eq. (4), one could simulate the transport properties of the GNR-based nanodevice without irradiation.

B. Electron-photon interaction

The term $H_{e\text{-ph},\sigma} = (\frac{e}{m_e})\vec{A} \cdot \vec{p}$ in Eq. (1) is the electron-photon interaction, where \vec{A} is the time-dependent electromagnetic vector potential, \vec{p} is the electron momentum operator, and m_e is the electron mass [9]. Optically induced spin and charge transports in the GNR channel, which is under the effect of E , were simulated using Eq. (4) together with the self-consistent solution of the total Green's function, expressed as [9]

$$G_{T,\sigma}(\varepsilon) = [G_{0,\sigma}^{-1} - \Sigma_{\text{ph},\sigma}]^{-1}. \quad (5)$$

The last term $\Sigma_{\text{ph},\sigma} = -\frac{i}{2}[\Sigma_{\text{ph},\sigma}^{\text{in}}(\varepsilon) + \Sigma_{\text{ph},\sigma}^{\text{out}}(\varepsilon)]$ in the equation above is the electron-photon self-energy for an

electron with the spin σ , where $\Sigma_{\text{ph},\sigma}^{\text{in}}$ and $\Sigma_{\text{ph},\sigma}^{\text{out}}$ are in-scattering and out-scattering self-energies due to the electron-photon interaction for α -spin and β -spin electrons, which can be expressed as [9,51]

$$\begin{aligned} \Sigma_{\text{ph},\sigma}^{\text{in}}(\varepsilon) &= (N_{\text{ph}} + 1)MG_{\sigma}^n(\varepsilon + \varepsilon_{\text{ph}})M^{\dagger} \\ &+ N_{\text{ph}}MG_{\sigma}^n(\varepsilon - \varepsilon_{\text{ph}})M^{\dagger}, \end{aligned} \quad (6)$$

$$\begin{aligned} \Sigma_{\text{ph},\sigma}^{\text{out}}(\varepsilon) &= (N_{\text{ph}} + 1)MG_{\sigma}^p(\varepsilon - \varepsilon_{\text{ph}})M^{\dagger} \\ &+ N_{\text{ph}}MG_{\sigma}^p(\varepsilon + \varepsilon_{\text{ph}})M^{\dagger}, \end{aligned} \quad (7)$$

where N_{ph} is the number of photons, $\varepsilon_{\text{ph}} = \hbar\omega$ is the photon energy, and the term M incorporates the electron-photon interaction, where each element is represented by [9,46]

$$M_{mn} = \langle m|A_0\hat{e} \cdot \vec{p}|n\rangle, \quad (8)$$

where A_0 is the amplitude of \vec{A} and \hat{e} denotes the light polarization. Furthermore, electron and hole correlation functions are described as

$$\begin{aligned} G_{\sigma}^n(\varepsilon) &= G_{\sigma}(\varepsilon)[\Gamma_{L,\sigma}(\varepsilon)f_L(\varepsilon) + \Gamma_{R,\sigma}(\varepsilon)f_R(\varepsilon) \\ &+ \Sigma_{\text{ph},\sigma}^{\text{in}}(\varepsilon)]G_{\sigma}^{\dagger}(\varepsilon), \end{aligned} \quad (9)$$

$$\begin{aligned} G_{\sigma}^p(\varepsilon) &= G_{\sigma}(\varepsilon)\{\Gamma_{L,\sigma}(\varepsilon)[1 - f_L(\varepsilon)] \\ &+ \Gamma_{R,\sigma}(\varepsilon)[1 - f_R(\varepsilon)] + \Sigma_{\text{ph},\sigma}^{\text{out}}(\varepsilon)\}G_{\sigma}^{\dagger}(\varepsilon), \end{aligned} \quad (10)$$

where $f_{L,R}$ and $\Gamma_{(L,R),\sigma}$ are the Fermi-Dirac function and the broadening function of the L/R semi-infinite GNR electrode. After calculating the electron-photon self-energy by self-consistently solving Eqs. (5)–(10), the spin-polarized photocurrent across the GNR-based nanodevice, can be obtained by [52]

$$\begin{aligned} I_{\text{ph},\sigma} &= \frac{2e}{h} \int d\varepsilon \text{Tr}\{G_{(1,1),\sigma}^p(\varepsilon)\Gamma_{L,\sigma}(\varepsilon)f_L(\varepsilon) \\ &- G_{(1,1),\sigma}^n(\varepsilon)\Gamma_{L,\sigma}(\varepsilon)[1 - f_L(\varepsilon)]\}, \end{aligned} \quad (11)$$

where h is the Planck's constant and $G_{(1,1),\sigma}^{n,p}(\varepsilon)$ are the first blocks of the electron and hole correlation functions [9,51]. To calculate the above equation, we neglected the spin-flipping and the spin-scattering, due to the long spin-relaxation length in graphene, which has been reported experimentally [53,54], micrometer-scale distances at room temperature. Moreover, as it has been shown experimentally [55], the length reveals presumably no dependence on device edges. Furthermore, the spin-flip scattering of electrons gliding along the ZGNR edges is very weak [56]. Therefore the spin-polarized carriers in ZGNRs can maintain their coherence for a relatively long time. Moreover, to assess the optical performance and the optically induced spin-filtering effect of the nanodevice, the spin-dependent quantum efficiency QE_{σ} and the optical spin polarization SP are defined, respectively, as

$$QE_{\sigma}(\%) = \frac{I_{\text{ph},\sigma}/e}{P_{\text{in}}/\hbar\omega} \times 100\% \quad (\sigma = \alpha, \beta), \quad (12)$$

$$SP(\%) = \frac{I_{\text{ph},\sigma} - I_{\text{ph},-\sigma}}{I_{\text{ph},\sigma} + I_{\text{ph},-\sigma}} \times 100\%, \quad (13)$$

where P_{in} is the incident optical power. All the calculations were performed at room temperature and the substrate effect was neglected because of the inversion-symmetry of the proposed substrate [57] and the absence of any staggered potential, as is present in the case of graphene/hBN or other substrates [9,57,58]. Since the spin-flip scattering is ignored, all transport equations must be decoupled into two independent components and must be separately solved for majority-spin (α -spin) and minority-spin (β -spin) electrons. For simulating the nanodevice based on NM AGNR under the effect of E , all calculations, including the electron-photon interaction, were performed independently of the spin degree of freedom, using the single-band tight-binding Hamiltonian. Therefore, in the latter case, the photocurrent is not spin-polarized and it does not possess any spin-filtering effect. Furthermore, in our designed nanodevice, the photocurrent is driven to the external circuit by applying a very small bias (0.01 V), without producing any accompanying dc dark current between the two electrodes, and thus the resulting current must have a pure photogenerated nature.

III. RESULTS AND DISCUSSION

Electric field induced properties of the designed nanodevice [shown in Fig. 1(a)] were simulated through the mean-field Hubbard approximation and the NEGF formalism by considering the simultaneous effect of irradiation and an external electric field. The incident illumination is assumed a polarized light spanned over a broad frequency range from THz to UV with the constant intensity of $I_\omega = 100 \text{ kW/cm}^2$, perpendicularly shed on top of the channel region. The electric field associated with the light is along the channel direction, as can be seen in Fig. 1(a). Moreover, a previous study [9] has revealed that the photocurrent depends on the polarization angle θ according to $\cos(2\theta + \varphi)$, where φ is a phase shift caused by the bias or the structural asymmetry of the system [9,59], which is approximately zero in our design that has the L-R symmetry due to the application of the same transverse electric field on both of its left and right electrodes under applying a small bias. Therefore, the selected polarization of the illumination leads to the maximum responsivity of the proposed spin-photovoltaic device. Furthermore, the GNR in the split-gate structure, producing a uniform external E across the GNR in the channel and along the lateral direction in the L/R electrode, as it is shown in Fig. 1(b) by a vertical arrow. Figure 1(b) shows the 6ZGNR, with a unit cell consisting of 12 atoms. First, we calculated the band structures of the GNRs in the absence and in the presence of E , without any illumination, to investigate the difference between the electronic structure of a pristine GNR and that of a GNR under an electric field. Second, having understood the electronic and spintronic properties, we calculated the photoresponsivity of the proposed nanodevice by shedding a linearly polarized light on the central region of the device. By properly tuning the incident photon energy, the electrons in the valence bands would be excited to the conduction bands and then the photocurrent can be flowed by applying a very small bias. Note that photocurrents are spin-polarized in the case of ZGNRs. Third, in the spin-dependent case, we calculated the degree of the spin polarization for the photogenerated

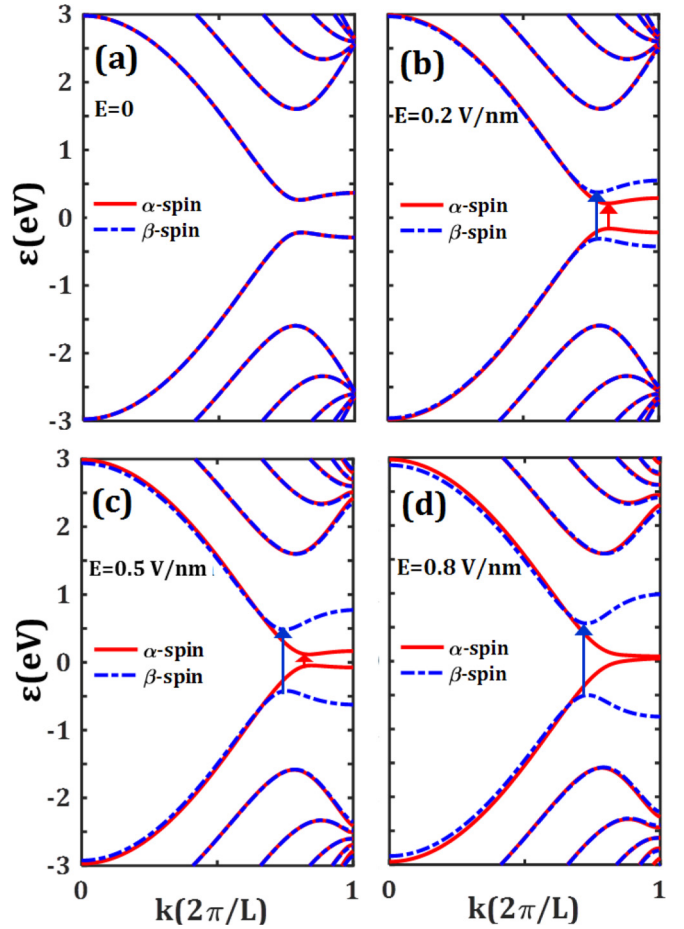


FIG. 2. Spin-resolved band structures of the ZGNR with (a) $E = 0$, (b) 0.2, (c) 0.5, and (d) 0.8 V/nm. The red (solid) and blue (dash-dotted) lines denote bands of α -spin and β -spin states, respectively. The first important allowable spin-conserved transitions (ε_F is set to zero).

carriers traversing along the channel region. For both of the ZGNR- and AGNR-based nanodevices, we supposed that the illuminated region consists of six unit cells.

A. ZGNR

Figure 2 shows the calculated spin-polarized band structures of the ZGNR around the Fermi level [the Fermi energy (ε_F) is set to zero] for various strengths of E . For $E = 0$ [Fig. 2(a)], consistent with previous studies [20,28], we found the AFM configuration as the ground state of the ZGNR with a FM ordering within each edge. This feature results from the breaking of the two-fold degenerate flat band at ε_F (when neglecting the spin degree of freedom) due to the electron-electron interaction [26,28], resulting in the lifting of the degeneracy between the valence and conduction edge states at ε_F and the revealing of the spin-degenerate band structure with a band gap of $\varepsilon_g \approx 0.48 \text{ eV}$ for 6ZGNR, which is consistent with the previous report [26]. Therefore, in the absence of E , irradiating photons of energies exceeding the ε_g will excite electrons of both spins from the occupied band to the unoccupied one and generate a photocurrent with no spin polarization. On the contrary, as shown in Figs. 2(b)–2(d)

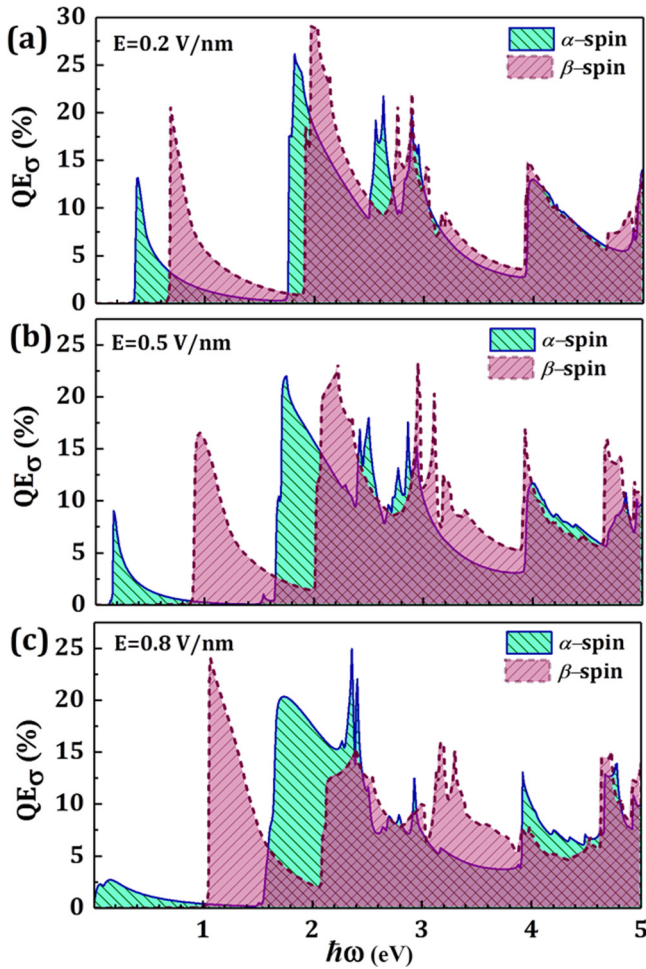


FIG. 3. Spin-dependent quantum efficiency as a function of the incident photon energy for the spin-photovoltaic device based on ZGNR under the simultaneous effect of linear illumination and a transverse electric field with the strength of (a) $E = 0.2$, (b) 0.5 , and (c) 0.8 V/nm.

and as we already know, the spin degeneracy is broken by applying the E and the spin-polarized band gap decreases for α -spin electrons while increases for β -spin electrons. As can be observed in Fig. 2, the extent of the band gap variation is straightforwardly related to the E strength; for example, for $E = 0.2$ and 0.5 V/nm for α -spin (β -spin) states, it is $\varepsilon_g^\alpha = 0.37$ eV ($\varepsilon_g^\beta = 0.68$ eV) and $\varepsilon_g^\alpha = 0.16$ eV ($\varepsilon_g^\beta = 0.9$ eV), respectively. Furthermore, the half-metallicity of the proposed nanodevice based on ZGNR is revealed at the critical strength of $E = 0.8$ V/nm, which closes the gap and leads to a metallic behavior for α -spin states, while the β -spin electrons show still a semiconducting behavior. Therefore, according to the mentioned band gaps, our designed spin-photovoltaic device could operate in a broad range of the electromagnetic spectrum, including the THz region, for $E > 0.5$ V/nm.

Now, we are going to examine the spin-photovoltaic properties of the ZGNR illuminated by a linearly polarized light with the photon energy of $\hbar\omega$ shed in the channel region. The quantum efficiency, which is spin-polarized, as a function of the photon energy is presented in Fig. 3. In this case, because of the spin splitting in the band structure of the

ZGNR, resulting from the applied E , by the absorption of light with an appropriate photon energy, the spin-polarized carriers with only one spin could be excited from the valence band to the conduction one, which results in the generation of a full spin-polarized photocurrent. As can be seen in Fig. 3(a) for the ZGNR under $E = 0.2$ V/nm, when the photon energy is 0.3 eV $< \hbar\omega < 0.6$ eV, the α -spin component of the photocurrent (I_{ph}^α) is nonzero, while the β -spin component is $I_{ph}^\beta \simeq 0$, producing a full and nearly full spin-polarized photocurrent in this photon energy range. Furthermore, the first spin-polarized absorption lines, with the quantum efficiencies of 21% and 13%, occur at $\hbar\omega = 0.39$ and 0.69 eV for α - and β -spin electrons, respectively. The first peak of the quantum efficiency for the α - (β -) spin component is consistent with the first allowable inter-band optical transition, which is shown in the band structure diagram with a red (blue) arrow (Fig. 2). Furthermore, the most allowable interband optical transitions, which are consistent with the maximum magnitude of the quantum efficiencies, occur in the visible (Vis) region with the magnitude of 26% (29%) for α - (β -) spin electrons. Note that, since there is no spin-flip interaction in the system, each of the spin-polarized absorption lines corresponds to a spin-conserved transition between the valence and conduction sub-states with the same spin characteristic. As can be observed in Fig. 3(b), under the electric field of $E = 0.5$ V/nm, one could see that the photoresponsivity begins at $\hbar\omega > 0.14$ eV in the THz region of the electromagnetic spectrum. Additionally, for the photon energy of $\hbar\omega < 0.8$ eV, we have approximately only I_{ph}^α with the maximum quantum efficiency of 10% in the THz region. Therefore, by increasing the strength of the electric field, we could achieve the THz photoresponsivity in the ZGNR with a full spin-polarized photocurrent. The most allowable spin-polarized optical transitions are also revealed in the Vis region with the quantum efficiencies of 22% and 23% for α - and β -spin electrons, respectively. By further increasing the electric field strength up to $E = 0.8$ V/nm [Fig. 3(c)], illuminating the channel with the photon energy of $\hbar\omega > 0$ results in the flowing of I_{ph}^α through the spin-photovoltaic device, which is due to the half-metallic behavior of this component. However, I_{ph}^β starts to appear above the threshold photon energy $\hbar\omega \approx 0.7$ eV, with the maximum quantum efficiency of 24% at $\hbar\omega = 1.07$ eV, which is also the first appeared quantum efficiency peak of this component.

To precisely clarify the spin-filtering effect of the proposed nanodevice in the wavelength region of the incident illumination, we showed the optical spin polarization of the ZGNR versus the photon energy in Fig. 4 for different strengths of the transverse electric field. As mentioned above, the spin splitting of the ZGNR band structures, due to the applied electric field, results in the appearance of the spin-polarized behavior of the nanodevice and especially, a fully spin-polarized photocurrent for only one spin component. This spin-filtering feature extends to different regions of the incident photon energy that belongs to the E strength. Consistent with the results of Fig. 3, Fig. 4 shows that increasing the strength of E decreases the threshold energy at which the full optical spin polarization starts. Interestingly, when the ZGNR is under $E = 0.8$ V/nm, one could see the full spin polarization emerging from $\hbar\omega > 0$, which is compatible with the half-metallic behavior of α -spin electrons. Furthermore, the range

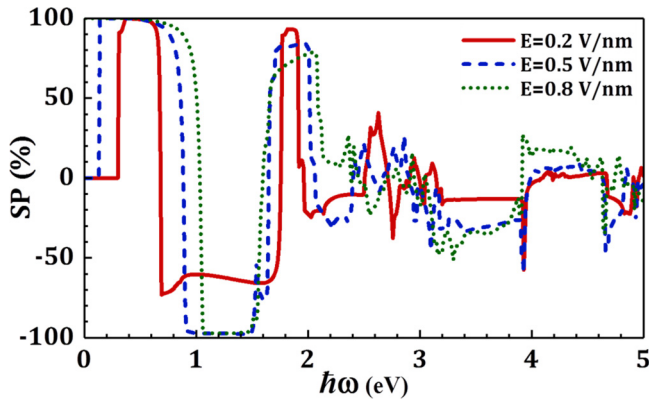


FIG. 4. The optical spin polarization of the proposed spin-photovoltaic device based on the ZGNR versus the photon energy for various E strengths.

of the full spin-polarized photoresponsivity widens as the electric field strength increases, which is considerable for optical spin-filtering and spin-valve applications. Generally, by properly tuning the external electric field, one is able to control the spin-polarized gap of the ZGNR and thus the range of the photoresponsivity of the proposed nanodevice, especially for low-energy applications operating in the THz region. On the other hand, strengthening E could improve the capability of the optical spin-filtering feature of our proposed nanodevice by broadening the full spin polarization region of the incident photon energy as well as by increasing the polarization magnitude.

B. ZGNR+defect

To estimate the effect of linear edge defects on the spin-photovoltaic responsivity of our proposed nanodevice, especially the robustness of the spin-polarized behavior for zigzag edges, we performed the calculations on a defective system [with a design shown in Fig. 5(a)]. Previous reports have shown the improvement of the GNR photoconductivity in infrared and THz regions due to the periodic defects introduced in an array structure [60]. The results show that even in the presence of linear edge defects, the qualitative electric field induced spin-polarized current remains for ZGNRs, although the strength of the spin-dependent photoresponsivity could be altered. As can be seen in Fig. 5(a), the proposed linear defects introduced along the two edges of the ZGNR are associated with no difference between the two sublattices of the bipartite system and thus do not deteriorate the AFM coupling of the nondefective GNR without any net magnetism. Therefore, one could expect a behavior similar to the spin-polarized behavior of the ZGNR under E , which is explained in Figs. 5(b) and 5(c) for $E = 0$ and $E = 0.2$ V/nm, respectively, and it is consistent with the previous report [35]. As can be observed in Fig. 5(b), the AFM band gap of the defective ZGNR is $\varepsilon_g \approx 0.16$ eV, which is lower than the pristine one due to the increased width of the GNR. Furthermore, applying a transverse electric field results in the splitting of α - and β -spin bands near the Fermi energy and also the increasing of the band gap belonging to β -spin states as $\varepsilon_g^\beta = 0.47$ eV. However, ε_g^α remains approximately invariant. In the case of

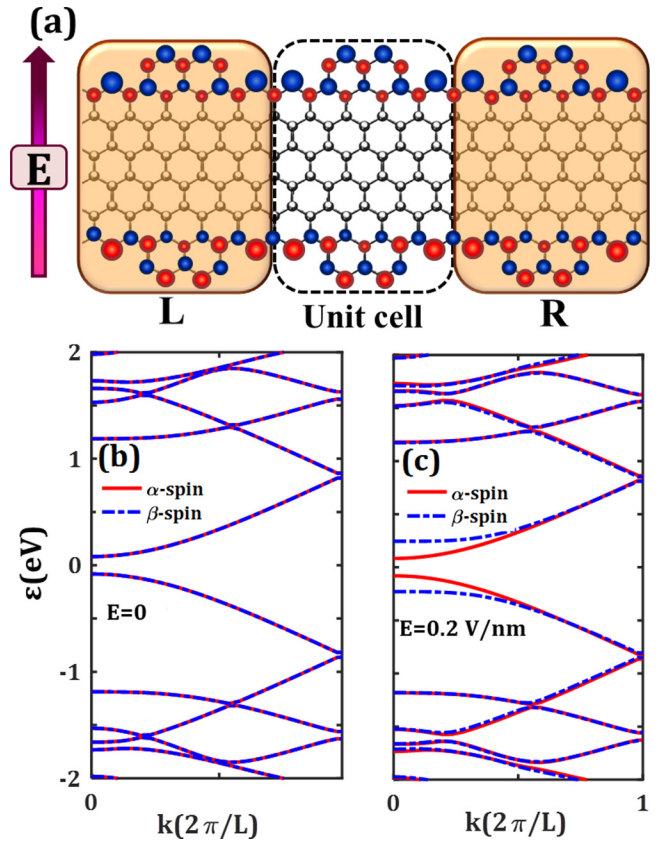


FIG. 5. (a) Schematic diagrams of the defective ZGNR under the effect of a transverse electric field. The rectangle box drawn with a dotted line denotes a supercell of the ZGNR. (b) and (c) show the spin-resolved band structures of the defective ZGNR with $E = 0$ and 0.2 V/nm, respectively. The red (solid) and blue (dash-dotted) lines denote the bands of α -spin and β -spin states, respectively.

ZGNRs with periodic edge defects, as opposed to the pristine ZGNR, wave functions belonging to valence and conduction band edges are distributed throughout the nanoribbon width [61]. Therefore the band gap does not vary sensitively by strengthening the electric field by more than 0.2 V/nm.

In order to compare the optical performance of the spin-photovoltaic device based on the nondefective ZGNR and the defective ZGNR, we presented in Fig. 6(a) the spin-dependent quantum efficiency of the defective ZGNR as a function of the photon energy under the effect of E . By comparing this figure with Fig. 3, one can see that the spin-dependent behavior of the photoresponsivity is preserved in the absence and the presence of the proposed edge defects. Furthermore, the qualitative behavior of the quantum efficiency diagram is the same, although the location and the height of the spin-dependent optical absorption lines could vary, which is attributed to the variation in the spin-resolved band structure and the appearance of different band gaps for α - and β -spin components, as compared to the non-defective GNR. As can be observed in Fig. 6(a), the first quantum efficiency peak of 5%, which is appeared at $\hbar\omega = 0.48$ eV, belongs to β -spin electrons; whereas the first optical absorption line of α -spin electrons, with the significant magnitude of 24%, occur for the second interband transition with $\hbar\omega = 1.28$ eV, and ε_g^α does

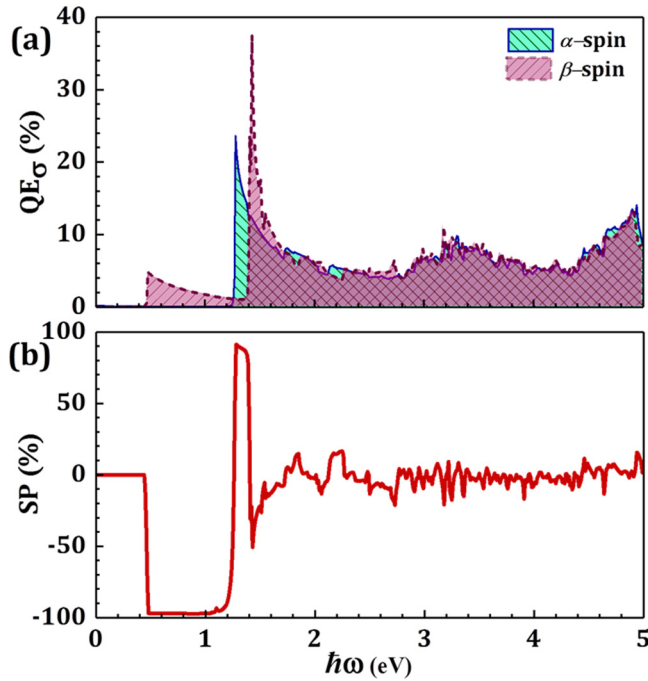


FIG. 6. (a) The spin-dependent quantum efficiency as a function of the incident photon energy for the spin-photovoltaic device based on the defective ZGNR under the simultaneous effect of linear illumination and the transverse electric field of the strength $E = 0.2$ V/nm. (b) The optical spin polarization of the proposed spin-photovoltaic device based on the defective ZGNR vs the photon energy for $E = 0.2$ V/nm.

not reveal any considerable quantum efficiency. Furthermore, to assess the role of the introduced edge defects on the electric field induced optical spin-filtering characteristic of the proposed device based on ZGNR, we calculated the optical spin polarization of the defective ZGNR taking into account the effect of E , and the results are presented in Fig. 6(b) for $E = 0.2$ V/nm. By comparing Fig. 6(b) with Fig. 4 for the device based on the pristine ZGNR without edge irregularities and the device based on the defective ZGNR, one can show that the region of the full optical spin polarization widens and extends to smaller photon energies for the defective one. Furthermore, Fig. 6(b) indicates that the introduction of the linear NM edge defects along a ZGNR could preserve the optical spin-filtering capability of the proposed nanodevice as well as reverse the polarization sign for $\hbar\omega < 0.7$ eV in the THz region. We found that the most excellent optical spin polarization for the defective ZGNR occurs under THz to infrared wavelengths, while the optical spin polarization is insignificant under Vis and UV wavelengths.

C. AGNR

In this section, we are going to focus on AGNRs and investigate their photoresponsivity and electric field modulated optoelectronic properties. As mentioned above, due to the NM characteristic of AGNRs, all their physical quantities, including the photocurrent, are independent of the spin degree of freedom. Therefore, by neglecting the electron-electron interaction, we simulated the proposed photovoltaic device

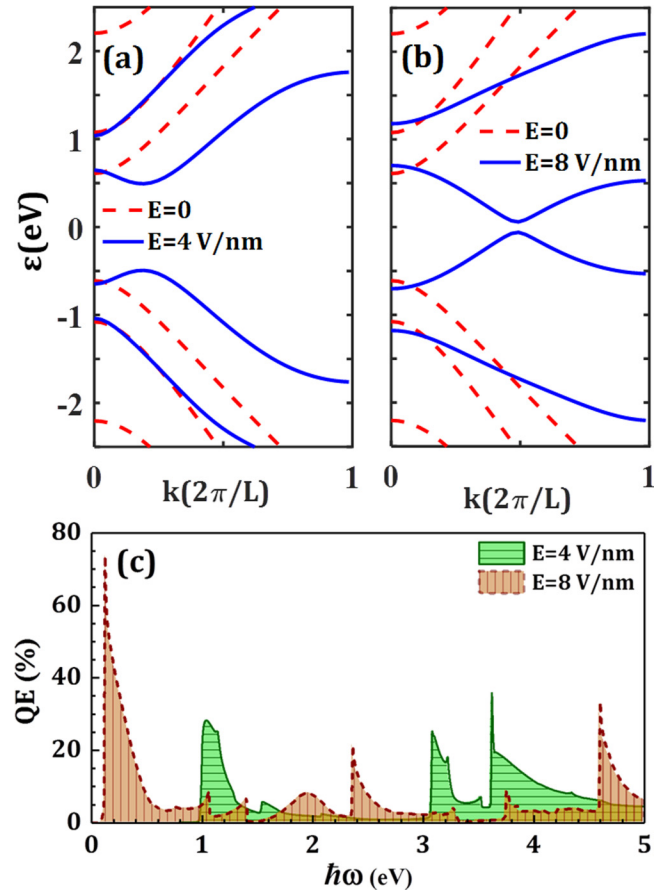


FIG. 7. [(a) and (b)] Band structures of AGNR with $E = 0, 4,$ and 8 V/nm (ϵ_F is set to zero). (c) Quantum efficiencies of the photovoltaic device based on AGNR as a function of the incident photon energy under the simultaneous effect of linear illumination and a transverse electric field.

based on 7AGNR using the tight-binding Hamiltonian and the NEGF formalism in the presence of E , with the numerical results shown in Fig. 7. 7AGNR ($n = 7$ indicates the number of dimer lines along the ribbon width) belongs to the subclass $3n + 1$ of AGNRs, with a semiconducting behavior and a larger band gap as compared to the two subclasses of $3n$ and $3n + 2$, with the latter revealing a semimetallic behavior. Furthermore, due to the more hybridization of wave functions, the rate of the perturbation effect and thus the variation in the band gap with E is larger as compared to the other two subclasses [30]. As can be observed in Figs. 7(a) and 7(b), although AGNR does not have any spin-dependent characteristic, its band structure could be still modulated with an external electric field applied along the lateral direction of GNR. By increasing the E strength, the band gap decreases monotonically and one could tune the band gap of an AGNR to a few $meVs$ by applying an appropriate electric field in the range of THz frequencies, which is achievable for $E = 8$ V/nm, as can be confirmed in Fig. 7(b). Figures 7(a) and 7(b) shows that the minimal band gap of AGNR moves towards the larger wave vector as the applied E increases. This feature, which is consistent with a previous work [31], could be attributed to the fact that the energy dispersion spectrum of

semiconducting AGNRs at the Γ point ($k = 0$) is unaffected by the electric field, while the other k points are affected by E .

Because of the NM behavior of the AGNR band structure and energy states, illuminating the channel region of the photovoltaic device based on AGNR with a properly tuned photon energy results in the absorption of the photons and the transition of the electrons from spin-less valence substates to conduction ones. This procedure leads to the generation of a photocurrent, which is independent of spin, and its flow under the very small bias of 0.01 V. We calculated the quantum efficiency from the photocurrent [shown in Fig. 7(c)] for $E = 4$ and 8 V/nm, with the latter one revealing the photoresponsivity in the THz region of incident photon energies. As can be observed in Fig. 7(c), the first allowable optical absorption line, whose location is consistent with the energy required for the first inter-band optical transition, moves to smaller photon energies as E increases. This peak is also the most probable one with the acceptable quantum efficiency as compared to the previous report [62]. Furthermore, although the maximum magnitude of the AGNR quantum efficiency is improved by strengthening the applied electric field, the localization and the clarity of the peaks are weakened. Note that a higher E strength is required to affect electronic and optoelectronic properties of the proposed nanodevice based on AGNR, including the proper tuning of the photoresponsivity in the THz region, as compared to the strength required for the ZGNR-based device. Finally, as stated before, GNRs with various structures, widths, and lengths can be obtained via different synthesis methods [11–14]. Furthermore, the realization of such an external electric field is possible experimentally, as performed in previous literatures [63–65].

IV. CONCLUSION

In summary, we studied the fully spin-polarized photocurrent induced by the terahertz to visible irradiation in a graphene nanoribbon through the application of an external transverse electric field (E), focusing on the modulation of the effects by tuning the field strength. Furthermore, by employing the self-consistent nonequilibrium Green's function (NEGF) formalism and the mean-field Hubbard model, we simulated the photoresponsivity of the spin-photovoltaic device based on pristine and defective GNRs under the monochromatic linearly polarized irradiation. In the case of ZGNRs, the degeneracy of the AFM band structure is split due to the applied E , and the splitting is tuned by varying the E strength to achieve the full and the nearly full spin-polarized photocurrent of ZGNR, especially in the THz region of the electromagnetic spectrum, which is important for a variety of applications [45]. On the other hand, the robustness of the spin-dependent behavior of our designed nanodevice based on ZGNRs was studied in the presence of edge defects, with the results revealing the spin-polarized photocurrent in photon energies ranging from THz to UV, with the reversing of the sign of the optical spin polarization in the THz to infrared range, as opposed to the pristine ZGNR. Finally, our simulation for the proposed nanodevice based on a semiconducting AGNR showed the tunability of its transport properties and its optical responsivity in the range of THz to UV wavelengths, by properly modulating the E strength, although it does not have any spin-dependent characteristic. Our approach may lead to a feasible possibility to develop all-carbon nanodevices with a broadband controllable photoresponsivity and a full spin-filtering feature, without involving any magnetic field or element.

-
- [1] S. Ganguly, M. Kabir, and T. Saha-Dasgupta, *Phys. Rev. B* **95**, 174419 (2017).
- [2] A. K. Geim and K. S. Novoselov, in *Nanoscience and Technology: A Collection of Reviews from Nature Journals* (World Scientific, Singapore, 2010), pp. 11–19.
- [3] X. Sun, S. Vélez, A. Atxabal, A. Bedoya-Pinto, S. Parui, X. Zhu, R. Llopis, F. Casanova, and L. E. Hueso, *Science* **357**, 677 (2017).
- [4] F. Ostovari and M. K. Moravvej-Farshi, *Appl. Phys. Lett.* **105**, 072407 (2014).
- [5] S. Zamani and R. Farghadan, *J. Phys. D* **51**, 305103 (2018).
- [6] H.-F. Lü, Y. Guo, X.-T. Zu, and H.-W. Zhang, *Appl. Phys. Lett.* **94**, 162109 (2009).
- [7] L. Zhang, K. Gong, J. Chen, L. Liu, Y. Zhu, D. Xiao, and H. Guo, *Phys. Rev. B* **90**, 195428 (2014).
- [8] S. Zamani and R. Farghadan, *Phys. Rev. Appl.* **10**, 034059 (2018).
- [9] X. Tao, L. Zhang, X. Zheng, H. Hao, X. Wang, L. Song, Z. Zeng, and H. Guo, *Nanoscale* **10**, 174 (2018).
- [10] K. Szałowski, *Phys. Rev. B* **90**, 085410 (2014).
- [11] J. Cai, P. Ruffieux, R. Jaafar, M. Bieri, T. Braun, S. Blankenburg, M. Muoth, A. P. Seitsonen, M. Saleh, X. Feng *et al.*, *Nature (London)* **466**, 470 (2010).
- [12] A. Radocea, T. Sun, T. H. Vo, A. Sinitskii, N. R. Aluru, and J. W. Lyding, *Nano Lett.* **17**, 170 (2016).
- [13] P. Ruffieux, S. Wang, B. Yang, C. Sánchez-Sánchez, J. Liu, T. Dienel, L. Talirz, P. Shinde, C. A. Pignedoli, D. Passerone *et al.*, *Nature (London)* **531**, 489 (2016).
- [14] T. H. Vo, M. Shekhirev, D. A. Kunkel, M. D. Morton, E. Berglund, L. Kong, P. M. Wilson, P. A. Dowben, A. Enders, and A. Sinitskii, *Nat. Commun.* **5**, 3189 (2014).
- [15] V. Barone, O. Hod, and G. E. Scuseria, *Nano Lett.* **6**, 2748 (2006).
- [16] L. Ponomarenko, F. Schedin, M. Katsnelson, R. Yang, E. Hill, K. Novoselov, and A. Geim, *Science* **320**, 356 (2008).
- [17] T. Mueller, F. Xia, and P. Avouris, *Nat. Photo.* **4**, 297 (2010).
- [18] F. Xia, T. Mueller, R. Golizadeh-Mojarad, M. Freitag, Y.-m. Lin, J. Tsang, V. Perebeinos, and P. Avouris, *Nano Lett.* **9**, 1039 (2009).
- [19] Z. F. Wang, S. Jin, and F. Liu, *Phys. Rev. Lett.* **111**, 096803 (2013).
- [20] Y.-W. Son, M. L. Cohen, and S. G. Louie, *Nature (London)* **444**, 347 (2006).
- [21] D. Wang, Z. Zhang, Z. Zhu, and B. Liang, *Sci. Rep.* **4**, 7587 (2014).

- [22] F. Donati, Q. Dubout, G. Autès, F. Patthey, F. Calleja, P. Gambardella, O. V. Yazyev, and H. Brune, *Phys. Rev. Lett.* **111**, 236801 (2013).
- [23] H. González-Herrero, J. M. Gómez-Rodríguez, P. Mallet, M. Moaied, J. J. Palacios, C. Salgado, M. M. Ugeda, J.-Y. Veillen, F. Yndurain, and I. Brihuega, *Science* **352**, 437 (2016).
- [24] J. Bhattacharjee, *J. Chem. Phys.* **137**, 094705 (2012).
- [25] C. Chakravarty, B. Mandal, and P. Sarkar, *Phys. Lett. A* **381**, 307 (2017).
- [26] J. Guo, D. Gunlycke, and C. White, *Appl. Phys. Lett.* **92**, 163109 (2008).
- [27] R. Maji and J. Bhattacharjee, *Sci. Rep.* **7**, 17094 (2017).
- [28] O. V. Yazyev, *Rep. Prog. Phys.* **73**, 056501 (2010).
- [29] Z. Wen-Xing, L. Yun-Xiao, T. Hua, X. Jun-Wei, and F. Lin, *Chin. Phys. B* **24**, 076104 (2015).
- [30] H. Raza and E. C. Kan, *Phys. Rev. B* **77**, 245434 (2008).
- [31] D. S. Novikov, *Phys. Rev. Lett.* **99**, 056802 (2007).
- [32] K. Majumdar, K. V. Murali, N. Bhat, and Y.-M. Lin, *Nano Lett.* **10**, 2857 (2010).
- [33] S. Lakshmi, S. Roche, and G. Cuniberti, *Phys. Rev. B* **80**, 193404 (2009).
- [34] J. Tuček, P. Błoński, J. Ugolotti, A. K. Swain, T. Enoki, and R. Zbořil, *Chem. Soc. Rev.* **47**, 3899 (2018).
- [35] G. Z. Magda, X. Jin, I. Hagymási, P. Vancsó, Z. Osváth, P. Nemes-Incze, C. Hwang, L. P. Biro, and L. Tapasztó, *Nature (London)* **514**, 608 (2014).
- [36] G. Tang, J. Zhou, Z. Zhang, X. Deng, and Z. Fan, *Carbon* **60**, 94 (2013).
- [37] G. Yin, Y. Liang, F. Jiang, H. Chen, P. Wang, R. Note, H. Mizuseki, and Y. Kawazoe, *J. Chem. Phys.* **131**, 234706 (2009).
- [38] V. Saroka, K. Batrakov, V. Demin, and L. Chernozatonskii, *J. Phys.: Condens. Matter* **27**, 145305 (2015).
- [39] V. Ilyasov, B. Meshi, V. Nguyen, I. Ershov, and D. Nguyen, *J. Chem. Phys.* **141**, 014708 (2014).
- [40] V.-T. Tran, J. Saint-Martin, and P. Dollfus, *Appl. Phys. Lett.* **105**, 073114 (2014).
- [41] A. V. Savin and Y. S. Kivshar, *Sci. Rep.* **7**, 4668 (2017).
- [42] H. Dong, F. Huang, and W. Xu, *Physica E: Low Dimens. Syst. Nanostruct.* **97**, 52 (2018).
- [43] C.-Y. Lin, T.-N. Do, Y.-K. Huang, and M.-F. Lin, *Optical Properties of Graphene in Magnetic and Electric Fields* (IOP Publishing, Bristol, UK, 2017).
- [44] V. Ryzhii and M. Ryzhii, *Phys. Rev. B* **79**, 245311 (2009).
- [45] L. Vicarelli, M. Vitiello, D. Coquillat, A. Lombardo, A. Ferrari, W. Knap, M. Polini, V. Pellegrini, and A. Tredicucci, *Nat. Mater.* **11**, 865 (2012).
- [46] M. Pourfath, *The Non-Equilibrium Green's Function Method for Nanoscale Device Simulation* (Springer, Wien, 2014).
- [47] R. Farghadan and E. Saievar-Iranizad, *J. Appl. Phys.* **111**, 014304 (2012).
- [48] M. Shirdel-Havar and R. Farghadan, *Phys. Rev. B* **97**, 235421 (2018).
- [49] S. Datta, *Quantum Transport: Atom to Transistor* (Cambridge University Press, Cambridge, 2005).
- [50] M. L. Sancho, J. L. Sancho, J. L. Sancho, and J. Rubio, *J. Phys. F* **15**, 851 (1985).
- [51] L. E. Henrickson, *J. Appl. Phys.* **91**, 6273 (2002).
- [52] M. Anantram, M. S. Lundstrom, and D. E. Nikonov, *Proc. IEEE* **96**, 1511 (2008).
- [53] C. Józsa, M. Popinciuc, N. Tombros, H. T. Jonkman, and B. J. van Wees, *Phys. Rev. Lett.* **100**, 236603 (2008).
- [54] N. Tombros, S. Tanabe, A. Veligura, C. Józsa, M. Popinciuc, H. T. Jonkman, and B. J. van Wees, *Phys. Rev. Lett.* **101**, 046601 (2008).
- [55] M. Popinciuc, C. Józsa, P. J. Zomer, N. Tombros, A. Veligura, H. T. Jonkman, and B. J. van Wees, *Phys. Rev. B* **80**, 214427 (2009).
- [56] V. K. Dugaev, E. Y. Sherman, and J. Barnaś, *Phys. Rev. B* **83**, 085306 (2011).
- [57] B. Huang, Q. Xu, and S.-H. Wei, *Phys. Rev. B* **84**, 155406 (2011).
- [58] M. M. Asmar, D. E. Sheehy, and I. Vekhter, *Phys. Rev. B* **95**, 241115(R) (2017).
- [59] Y. Xie, L. Zhang, Y. Zhu, L. Liu, and H. Guo, *Nanotechnology* **26**, 455202 (2015).
- [60] Y. Zhang, T. Liu, B. Meng, X. Li, G. Liang, X. Hu, and Q. J. Wang, *Nat. Commun.* **4**, 1811 (2013).
- [61] H. Raza, in *Graphene Nanoelectronics* (Springer, Berlin, Heidelberg, 2011), pp. 529–553.
- [62] F. Ostovari and M. K. Moravvej-Farshi, *J. Appl. Phys.* **120**, 144505 (2016).
- [63] Y. Zhang, T.-T. Tang, C. Girit, Z. Hao, M. C. Martin, A. Zettl, M. F. Crommie, Y. R. Shen, and F. Wang, *Nature (London)* **459**, 820 (2009).
- [64] N. Jiang, Y. Zhang, Q. Liu, Z. Cheng, Z. Deng, S. Du, H.-J. Gao, M. Beck, and S. Pantelides, *Nano Lett.* **10**, 1184 (2010).
- [65] E. Gruber, R. A. Wilhelm, R. Pétuya, V. Smejkal, R. Kozubek, A. Hierzenberger, B. C. Bayer, I. Aldazabal, A. K. Kazansky, F. Libisch *et al.*, *Nat. Commun.* **7**, 13948 (2016).